Chapter 4 – Metallic Glasses as Shielding for Hypervelocity Impacts

As human activity has increased in low-earth orbit, so has the accumulation of space debris and the corresponding hazard to space vehicles.[1–3] From 1960 to 1996, the number of objects in orbit increased linearly at a rate of approximately 250 objects per year.[2] Since 1996, however, the number of objects in orbit has been increasing exponentially due to a combination of low-cost space technology and a large number of nations launching spacecraft and satellites. The primary hazard to space vehicles from micrometeoroid and orbital debris (MMOD), comprising fragmentation debris, spacecraft, rocket bodies, and operation debris, is the kinetic energy of these masses traveling at hyper velocities (5-15 km/s).[1–6]

Large debris, generally considered to be objects larger than 100 mm in diameter, can be tracked and characterized by ground-based radar for attitude, size, shape, orbital lifetime, ballistic coefficient, and mass.[2] An impact with large debris is catastrophic for most space vehicles, and collision avoidance maneuvers have been used in the past by the Space Shuttle, satellites, and the International Space Station to prevent such an occurrence.[3] Conversely, small debris projectiles, too small to detect and avoid, have already caused damage to operational space systems.[2] To mitigate the risk of loss of function or mission failure from small debris collisions, particularly from 1 to 5 mm diameter particles, spacecraft designers incorporate implicit protection into vehicle architecture, and explicit MMOD shield impact protection concepts.[5]

A range of shield concepts, including single metal sheets, complex layers of metal, carbon composites, fabrics, and honeycomb sandwich panels (HSPs), have been studied and implemented into space vehicles to mitigate the risk of MMOD impacts.[3–7] The most common type of shield, developed by Fred Whipple in the 1940s, consists of multiple layers separated by a gap, called a standoff (Figure 4-1). The front face sheet of the shield is called the "bumper" and the rear face sheet is called the "rear wall." The bumper breaks up the impacting particle into a spray of melt and vapor that expands while moving though the standoff. Dispersion of the debris cloud over a wider area of the rear wall helps prevent perforation or detached spall. Successful operation of the shield requires that the rear wall survive the impact. The performance of MMOD shields is often estimated using computer simulations and hydrocodes (a computer program used to model the fluid flow of a system) developed from ballistic limit equations (BLEs) obtained via hypervelocity testing.[5–13] For a given shield configuration, test variables include projectile size, velocity, density, and impact angle. The data obtained from a hypervelocity test program are then used to statistically predict the performance of a shield and establish design parameters. For example, the minimum thickness (t_{Ti}, cm) of a titanium wall to prevent a given amount of damage is given by the empirical BLE: [57]

$$t_{Ti} = 5.24d \cdot K \cdot BHN^{-0.25}\left(\frac{\rho_p}{\rho_t}\right)^{\frac{1}{2}}\left(\frac{V\cos\theta}{C_t}\right)^{\frac{2}{3}} \tag{1}$$

where d is the projectile diameter (cm), K the damage parameter for titanium (1.8 for perforation, 2.4 for detached spall, or 3 for incipient attached spall), BHN the Brinell hardness of the target, ρ_p the density of the projectile and ρ_t the density of the target (g/cm³), C_t the speed of sound in the target (km/s), V the projectile velocity (km/s), and θ is the impact angle from target normal. Thus, a single wall of Ti-15-3-3-3 must be at least 2 mm thick to prevent detached spall from the impact of a 0.8 mm aluminum projectile impacting normal to the plate at a velocity of 6.4 km/s. Equation (1) for titanium shields demonstrates that the material properties which have the most effect on ballistic performance are the hardness and density of the shield (and to a lesser extent, the speed of sound in the target). Subsequently, by increasing the hardness and density of the shield material, the minimum thickness of the shield to prevent a given amount of damage decreases. The density, diameter, and velocity of the projectile also dramatically affect damage, but these parameters cannot be controlled during a real MMOD impact event. Lastly, the impact angle of the projectile affects the ballistic performance of a shield. A normal impact is expected to cause the most damage, while a glancing (oblique) impact does the least damage. Although the trajectory of the projectile cannot be controlled, the design of the shield's surface morphology can affect the impact angle.

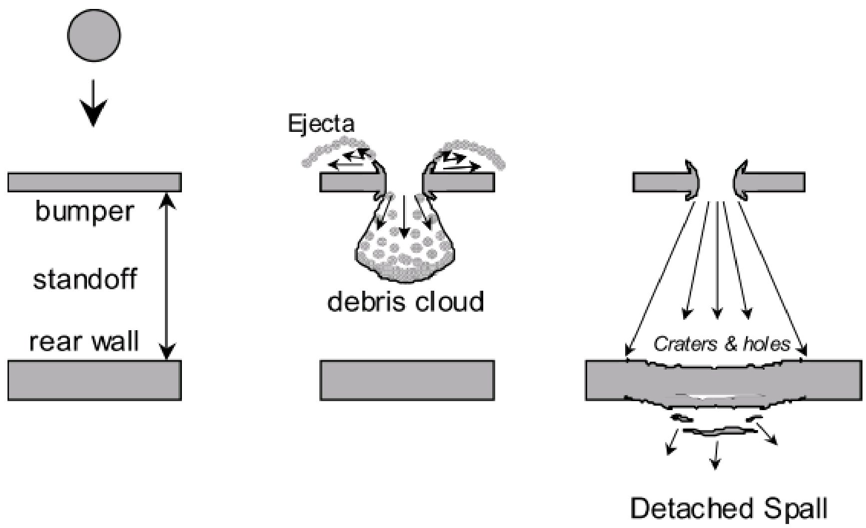

Figure 4-1: A schematic of a Whipple shield with a front bumper, empty space, and a rear wall to catch debris. (b) Impacts will create a cloud of debris both forwards and backwards. (c) If the debris cloud is not sufficiently diffuse it can result in either further penetration or detached spall from the rear wall. Image from Reference [5].

Although BLEs are empirical for each material (Table 4-1), trends in the performance of aluminum, titanium, and steel shields are useful for designing shields from new materials. For example, an optimal bumper shielding material, which combines performance with overall cost, is one that has an extremely high hardness and density, with a multi-faceted face sheet that turns a normal impact into an oblique one, while an optimal foam shield would have a cellular structure that diffuses the impact angle, disperses the debris cloud, and minimizes the shield system of mass. While high hardness would imply that a ceramic shield would be optimal, their high melting temperatures prevent vaporization during MMOD impacts. Solid matter passing through the outer shield, as opposed to liquid and vapor, threatens the spacecraft wall. A truly optimal bumper material combines high hardness and low density with low-melting temperature. This way an MMOD impact vaporizes both the projectile and shield. If the shield is not vaporized it can contribute to the debris cloud impacting the rear wall.

Table 4-1: Ballistic limit equations for various materials	
Material	Thickness to prevent damage
Titanium Alloys	$t_{Ti} = 5.24d \cdot K \cdot BHN^{-0.25}\left(\frac{\rho_p}{\rho_t}\right)^{\frac{1}{2}}\left(\frac{V\cos\theta}{C_t}\right)^{\frac{2}{3}}$
Steel	$t_{Steel} \geq 0.781d^{19/18}\left(\frac{\rho_p}{\rho_p}\right)^{1/2}(V\cos\theta)^{2/3}$
Aluminum Alloys	$t_{Al} = 15.72d^{19/18}BHN^{-0.25}\left(\frac{\rho_p}{\rho_t}\right)^{2/3}\left(\frac{V\cos\theta}{C_t}\right)^{2/3}$
d = projectile diameter (cm); P_x = penetration depth in semi-infinite target of material x (cm); $\rho_{p\,=}$ projectile density (g/cm^3); ρ_t = target density (g/cm^3); $t_{Material}$ = thickness of steel target (cm); θ = impact angle from target normal; θ = 0° impact normal to target; V = projectile velocity (km/s), BHN is the Brinell Hardness number, C_t = speed of sound in target	

Using these shield design criteria, bulk metallic glasses (BMG) and BMG-based matrix-composites (BMGMC) are strong candidates for bumper shielding. BMGMCs are ideal due to their similar density to titanium alloys (5.1-5.8 g/cm^3 vs. 4.5-4.5 g/cm^3, respectively), but they have more than twice the hardness (600 BNH vs. 250 BNH, respectively). They are also designed around deep eutectics to provide a low melting temperature (~900 K) which allows for greater ease of vitrification.[14] The low-solidus temperature and high viscosities of BMGMCs also enable unique panel fabrication methods. As shown in the previous chapter, semi-solid forging techniques have been developed previously to fabricate thin (<0.8 mm wall thickness) panels of BMGMCs in an “eggbox” configuration.[15] These panels exhibit superior specific energy absorption values for cellular structures due to advantageous combinations of high strength, high ductility, and low relative density. These structures also present a multi-faceted surface to an incoming projectile, ensuring that the impact angle is always near 45°. These combinations of features are investigated in the current chapter.

Thin panels of BMGMCs were subjected to hypervelocity impacts at the NASA Ames Vertical Gun Range using a two-stage light gas gun capable of firing a variety of projectiles from a sabot at velocities from 0.8 to 5.5 km/s (Figure 4-2a). BMGMCs plates were fabricated by semi-solid forging.[16] The alloy was heated by induction to a temperature between the solidus and liquidus (~1225 K), held isothermally to allow the microstructure to coarsen, and then forged using water cooled copper molds (Figure 4-2b and 4-2d). DH1 ($Zr_{36.6}Ti_{31.4}Nb_7Cu_{5.9}Be_{19.1}$) BMGMC[17] was used in the forging of thin plates (0.5-1.0 mm thick) from 10 g ingots, Figure 4-2c, and thin eggbox panels (0.6 mm nominal wall thickness) from 25 g ingots (Figure 4-2e). The nominal microstructure from each alloy is shown in the inset of Figure 4-2e. The lighter contrast material is the coarsened dendrites and the darker material is the metallic glass matrix. The panels were fastened to a testing jig, Figure 4-2f, and impacted at a normal angle, with velocities ranging from 0.8 to 3.0 km/s, using 3.17 mm aluminum spheres packed in a sabot. The charges were ignited using gunpowder and the sabot was stripped off immediately after the sphere left the gun barrel. The velocity was measured using time-of-flight between sensors and the impact was captured using three laser-triggered cameras. Three cameras recorded each impact: a backlit one using 500,000 frames per second, another using 1,000,000 frames, while a third was

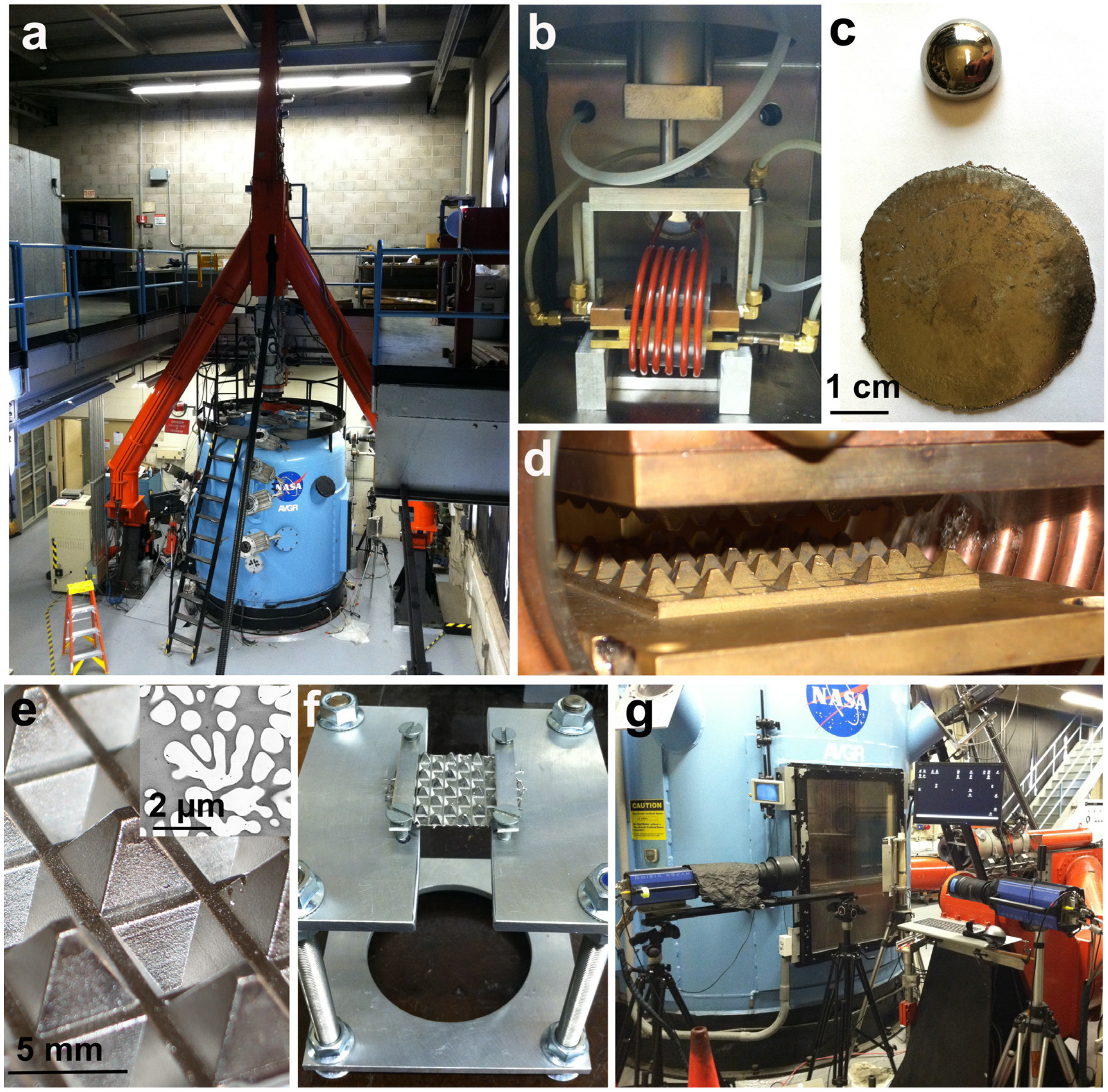

Figure 4-2: Hypervelocity facility and test samples – (a) View of the NASA Ames Vertical Gun Range, which consists of a two-stage light gas gun capable of firing projectiles in two different configurations to allow simulations of impacts from 0.8 to 5.5 km/s. The environmental test chamber is over 2 m high and the angle of impact can be changed using multiple ports on the side. (b) Forging chamber used to fabricate thin plates and eggbox structures. (c) Example of a 10 g ingot of the BMGMC DH1 ($Zr_{36.6}Ti_{31.4}Nb_7Cu_{5.9}Be_{19.1}$) forged into a 0.8 mm thick sheet. (d) Mold used to forge eggbox panels from BMGMCs. (e) BMGMC eggbox with a 0.6 mm thick wall semisolidly forged and the nominal microstructure shown in the inset. (f) Eggbox panel fixed to testing jig. The hole in the bottom plate allows for the collection of debris from the impact. During some impacts, a witness plate was used instead to assess damage. (g) Setup of the high-speed cameras used to capture the impact. Three cameras can be seen in the image (one is at the upper right).

left with an open shutter to collect all the light emitted from the event. The setup is shown in Figure 4-2g.

Figure 4-3 shows two hypervelocity impacts from 3.17 mm spherical aluminum projectiles flying at 2.3 km/s to contrast the performance of a BMGMC shield in different geometries (a thin plate and a multi-faceted eggbox). Six images captured in sequence during impact testing of the eggbox structure are exhibited in Figure 4-3a. The view is edge-on and backlit. The clamping screws are visible at the top and bottom of the sample. The impact occurred on a 45° angled surface of the eggbox, and the event took ~102 μs from the initial impact to the dissipation of the energy releasing flash. Similar impact conditions were used for a thin plate of the same BMG composite with approximately the same thickness, but in a flat configuration instead of the multi-faced one, and results are exhibited in Figure 4-3b. In comparison to the eggbox geometry, the flat plate has a much shorter energy-release flash and the debris cloud is much less diffuse as it travels down range. An estimation of the energy dissipated as light was obtained by counting the white pixels in each frame of video and plotting it versus the frame number (Figure 4-3c). The eggbox geometry produced a light intensity over four times greater than the flat plate as seen when analyzing the non-backlit camera (which is set up to capture only light intensity). Moreover, the eggbox effectively diffused the debris cloud after the impact. Image analysis of at least 95% of the debris cloud was used to estimate the dispersion angle (Figure 4-3d and 4-3e). The dispersion angle of the debris cloud was increased substantially by faceting the surface, from 76° to 101° for flat and faceted surfaces, respectively. Figure 4-3f and 4-3g show a time lapse image of the entire impact taken from a camera above the samples, where all of the light generated in the image is from the impact (the red light is an LED that backlights the samples and pulses at the same frequency as the high speed camera,

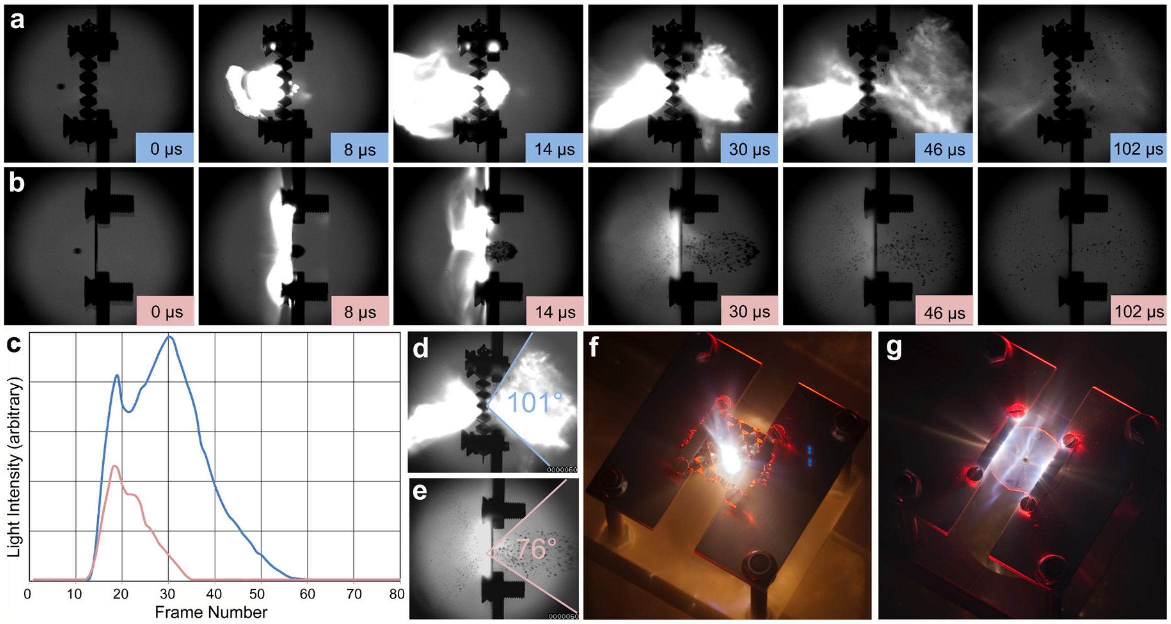

Figure 4-3: Comparison of surface geometry during hypervelocity impacts in BMG composite panels. (a) Backlit side-view images from a 3.17 mm aluminum sphere impacting a 0.6 mm thick DH1 eggbox, shown in (c), at 2.7 km/s for the first 102 µs after impact. The multi-faceted surface effectively diffuses the impact into a broad debris cloud. (b) The same velocity impact as (a) into a 0.7 mm thick BMGMC composite sheet. The impact conditions and alloy are the same between (a) and (b) but the surface geometry is different. In (b) the debris cloud is tightly clustered after impact. (c) Plot of light intensity versus frame number for the hypervelocity tests in (a,b). As an estimation of energy released during impact, image analysis was used to determine the length and intensity of the light. The eggbox is much more effective than the thin sheet at dissipating energy. (d,e) Image analysis was used to designate a range of angle of the debris cloud that captures at least 95% of the debris. The eggbox geometry (d) has a 25° wider spread than the thin sheet (e). (f,g) Long exposure images from the impacts in the eggbox (f) and the thin sheet (g) illustrating the difference in light intensity during the impact. The red light is the laser used to trigger the high-speed camera.

500 KHz). The single wall impact demonstrates the advantages of the thin, multi-faceted eggbox geometry to diffuse debris from the initial impact.

Cellular geometries have previously been employed for MMOD shielding. Specifically, aluminum honeycomb sandwich panels (HSPs) have been used widely as spacecraft shielding due to their low-areal density and ability to diffuse MMOD impacts because of the cellular geometry. HSPs are generally brazed to aluminum facesheets to form the shield, and their performance in hypervelocity tests is well established.[3,6,8,9] These shields exhibit drawbacks, however, including low hardness of the aluminum facesheets, a channeling effect during impacts caused by the honeycomb geometry that prevents dispersion of the debris cloud, low intrinsic strength, and difficulties with brazing. A more effective metal cellular shield can be created by using a harder and higher strength metal and making the geometry stochastic (e.g., using random bubbles instead of tubular honeycombs). The challenge, however, is that these types of cellular structures are difficult to fabricate from conventional high strength metal alloys, such as titanium and steel, due to the higher processing temperatures required to form them. Earlier in this thesis it was shown that bulk metallic glass matrix composites can be welded together via capacitive discharge. Figure 4-4a-d illustrates this method. A welded 6x6x3 cellular structure is shown in Figure 4-4e. It is fixed into the testing jig in Figure 4-4i. For comparison, an aluminum HSP with its upper face sheet removed is provided in Figure 4-4f. In the HSP, impact debris is able to pass through the honeycomb structure easily, an effect called "channeling." In the BMG composite egg-box structure, debris must perforate each multi-faceted layer of the egg-box to penetrate the structure.

Hypervelocity testing was performed on the three-layer BMG composite egg-boxes by firing a 3.17 mm aluminum sphere at 2.3 km s^{-1}, as shown in Figure 4-4g. The projectile impacted an angled surface at 45°, similar to the single layer test, and the debris diffused between the first and second layer. The debris moved laterally in the fifth frame, and then dissipated out the top and bottom, and only a small region of detached spall reached the third layer. The welded

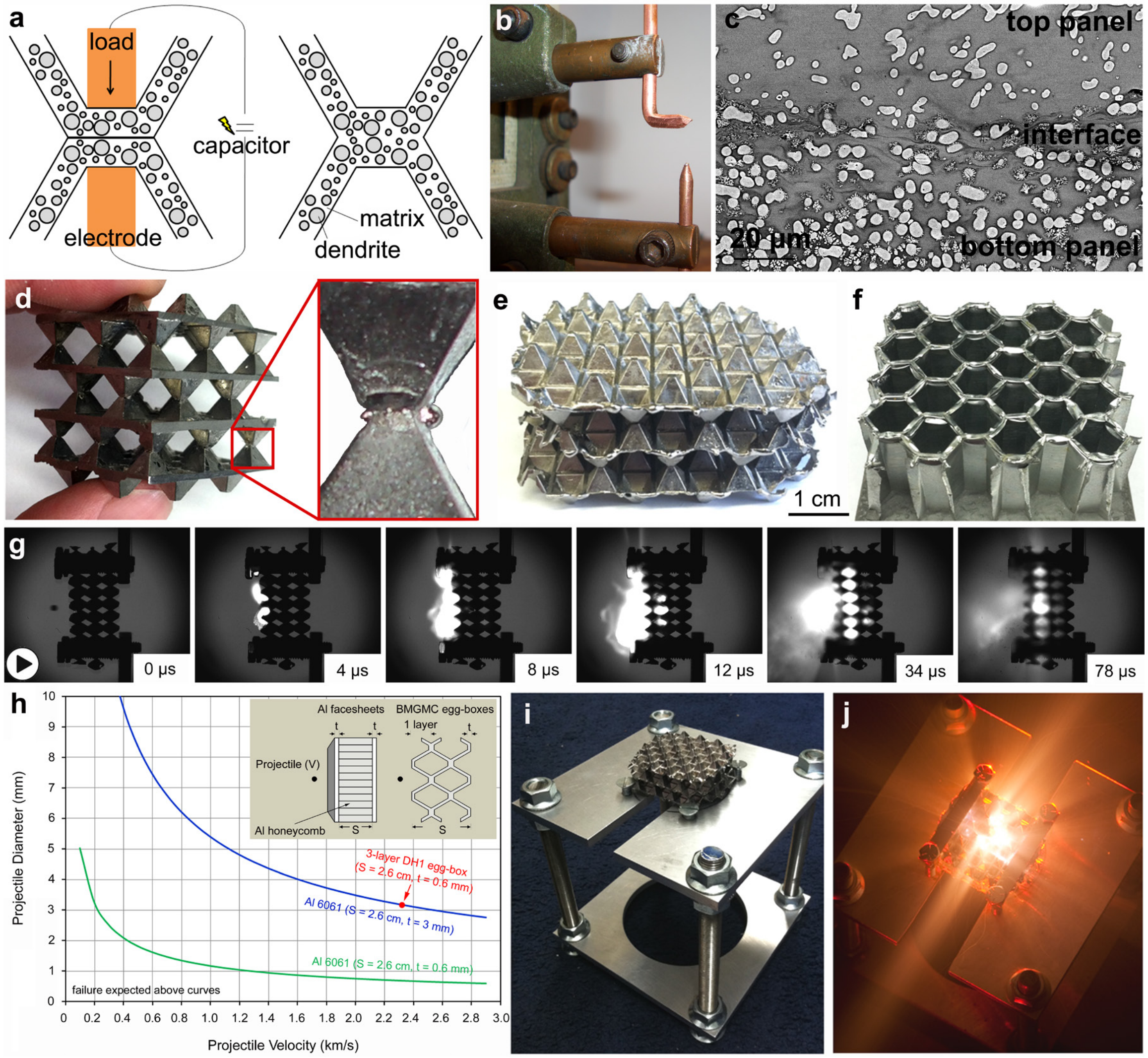

Figure 4-4: Hypervelocity impact of a welded BMG composite cellular structure. (a) Schematic of the capacitive joining process for a BMG composite. (b) Shaped electrons on a spot welder were used to weld egg-boxes together. (c) SEM micrograph from two egg-box panels welded together. (d-e) Egg-box panels which have been welded together. (f) Aluminum HSP structure. (g) Backlit side view of the three layer egg-box structure being impacted by a 3.17 mm aluminum projectile at 2.3 km s^{-1} showing penetration of the first layer and slight penetration of the second layer. (h) Plot showing projectile diameter versus projectile velocity for aluminum sandwich panels with aluminum facesheets calculated from ballistic limit software. S is the height of the honeycombs and t is the thickness of the face sheets. (i) The layered egg-box structure loaded into the sample holder. (j) A long exposure image showing the light generated during the hypervelocity impact.

joints remained intact throughout the impact, and the kinetic energy of the projectile was mitigated. Figure 4-4h shows a plot of BLEs for aluminum HSPs provided by NASA's Johnson Space Center. The lower green curve represents aluminum HSP with the same overall thickness as the three layered BMG structure (26 mm), and with face sheets equal in thickness to the wall of the BMG structure (0.6 mm). The performance of the three layered BMG composite structure falls on the BLE for an aluminum HSP with thickness of 26 mm, but with much thicker face sheets (3 mm vs. 0.5 mm in the composite). Because the third layer of the BMG composite cellular structure was not perforated, the BLE for this structure lies above the upper blue curve in Figure 4-4e. A long exposure image of the entire impact is shown in Figure 4-4j.

This chapter involved a preliminary assessment of BMG composites as potential spacecraft shielding against the threat of MMOD. Utilizing known parameters obtained from hypervelocity testing of conventional materials, BMG composite shield concepts were designed to exploit the critical material and geometric properties (mainly hardness, density, and impact angle) and tested using hypervelocity impacts. We demonstrated that welded panels of BMG composites offer a unique shielding solution for future satellites and spacecraft that are increasingly exposed to the threat of MMOD collisions. This work was also a collaboration with Professor Steve Nutt and Marc Davidson of USC, who assisted in the analysis of the debris cloud.

References

(1) Debris, O.; Committee, T. A.; Debris, S.; Isbn, C.; Pdf, T.; Press, N. A.; Academy, N. *Orbital Debris: A Technical Assessment*; National Academy Press: Washington, DC, 1995; p. 224.

(2) Space, S. and T. S. of the U. N. C. on the P. U. of O. *Technical Report on Space Debris*; United Nations: New York, 1999.

(3) Christiansen, E. L.; Nagy, K.; Lear, D. M.; Prior, T. G. Space station MMOD shielding. *Acta Astronaut.* **2009**, *65*, 921–929.

(4) Schonberg, W. P. Protecting Earth-orbiting spacecraft against micro-meteoroid/orbital debris impact damage using composite structural systems and materials: An overview. *Adv. Sp. Res.* **2010**, *45*, 709–720.

(5) Christiansen, E. L. *Handbook for Designing MMOD Protection*; National Aeronatuics and Space Administration Johnson Space Center: Houston, TX, 2009; p. 152.

(6) Destefanis, R.; Schäfer, F.; Lambert, M.; Faraud, M. Selecting enhanced space debris shields for manned spacecraft. *Int. J. Impact Eng.* **2006**, *33*, 219–230.

(7) Ryan, S.; Christiansen, E. L. *Micrometeoroid and Orbital Debris (MMOD) Shield Ballistic Limit Analysis Program*; TM-2009th–21st ed.; National Aeronautics and Space Administration Johnson Space Center: Houston, TX, 2010.

(8) Sibeaud, J.-M.; Thamié, L.; Puillet, C. Hypervelocity impact on honeycomb target structures: Experiments and modeling. *Int. J. Impact Eng.* **2008**, *35*, 1799–1807.

(9) Schonberg, W.; Schafer, F.; Putzar, R. Hypervelocity impact response of honeycomb sandwich panels. *Acta Astronaut.* **2010**, *66*, 455–466.

(10) Grujicic, M.; Pandurangan, B.; Zhao, C. L.; Biggers, S. B.; Morgan, D. R. Hypervelocity impact resistance of reinforced carbon–carbon/carbon–foam thermal protection systems. *Appl. Surf. Sci.* **2006**, *252*, 5035–5050.

(11) Yang, C.; Liu, R. P.; Zhan, Z. J.; Sun, L. L.; Wang, W. K. High speed impact on Zr41Ti14Cu12.5Ni10Be22.5 bulk metallic glass. *Mater. Sci. Eng. A* **2006**, *426*, 298–304.

(12) Hayhurst, C. J.; Livingstone, I. H. G.; Clegg, R. A.; Destefanis, R.; Faraud, M. Ballistic limit evaluation of advanced shielding using numerical simulations. *Int. J. Impact Eng.* **2001**, *26*, 309–320.

(13) Yang, C.; Wang, W. K.; Liu, R. P.; Liu, L.; Zhang, X. Y.; Li, L. X. Impacted by Hypervelocity Projectiles. *J. Spacecr. Rockets* **2006**, *43*, 12–14.

(14) Johnson, W. L. Bulk glass-forming metallic alloys: science and technology. *MRS Bull.* **1999**, *24*, 42–56.

(15) Schramm, J. P.; Hofmann, D. C.; Demetriou, M. D.; Johnson, W. L. Metallic-glass-matrix composite structures with benchmark mechanical performance. *Appl. Phys. Lett.* **2010**, *97*, 241910.

(16) Hofmann, D. C.; Kozachkov, H.; Khalifa, H. E.; Schramm, J. P.; Demetriou, M. D.; Vecchio, K. S.; Johnson, W. L. Semi-solid induction forging of metallic glass matrix composites. *JOM* **2009**, *61*, 11–17.

(17) Hofmann, D. C.; Suh, J.-Y.; Wiest, A.; Duan, G.; Lind, M.-L.; Demetriou, M. D.; Johnson, W. L. Designing metallic glass matrix composites with high toughness and tensile ductility. *Nature* **2008**, *451*, 1085–9.